CHEMICAL REVIEWS

pubs.acs.org/CR

Review

Rotating Frame Relaxation in Magic Angle Spinning Solid State NMR, a Promising Tool for Characterizing Biopolymer Motion

Eric G. Keeler and Ann E. McDermott*

Cite This: *Chem. Rev.* 2022, 122, 14940−14953

Read Online

ACCESS | Metrics & More | Article Recommendations

ABSTRACT: Magic angle spinning NMR rotating frame relaxation measurements provide a unique experimental window into biomolecules dynamics, as is illustrated by numerous recent applications. We discuss experimental strategies for this class of experiments, with a particular focus on systems where motion-driven modulation of the chemical shift interaction is the main mechanism for relaxation. We also explore and describe common strategies for interpreting the data sets to extract motion time scale, activation energy, and angle or order parameters from rotating frame relaxation data. Using model free analysis and numerical simulations, including time domain treatment, we explore conditions under which it is possible to obtain accurate and precise information about the time scales of motions. Overall, with rapid technical advances in solid state NMR, there is a bright future for this class of studies.

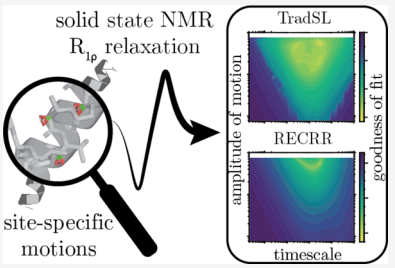

CONTENTS

1. INTRODUCTION

Understanding biopolymer thermal motions is central to the structure−function relationship. Essentially, all macromolecular

Received: June 25, 2022
Published: September 13, 2022

https://doi.org/10.1021/acs.chemrev.2c00442
Chem. Rev. 2022, 122, 14940−14953

properties of interest from binding thermodynamics to catalysis mechanisms require fluctuations, and therefore prediction of these functional properties has required knowledge of biopolymer dynamics. Nuclear magnetic resonance, including measurements in solution and the solid state, has been a powerful experimental tool for probing biopolymer dynamics on time scales from minutes to picoseconds. Experimental strategies for characterizing dynamics using solid state NMR have been a particularly active area of research recently.[1−4]

We explore the case of rotating frame relaxation measurements with magic angle spinning, which have developed into the technique du jour for studying microsecond-to-millisecond motions, encompassing many events of great functional importance such as binding-related rearrangements and allosteric responses.[5] In these experiments, conformational exchange processes cause large fluctuations in chemical shifts, dipolar couplings, and other local anisotropic interactions since the motions generally change the angle of the functional group with respect to the applied static field. Also, the changes in the local environment associated with conformation exchange can lead to additional (typically smaller) changes in shifts and couplings, analogous to the case for exchange detected by solution NMR. Fluctuations in local interactions in turn lead to the decay of nonequilibrium transverse magnetization. In these experiments, magnetization is first prepared by flipping it from its equilibrium position along z to an orthogonal direction (or sometimes a nonorthogonal but nonequilibrium direction when performing off-resonance $R_{1\rho}$ experiments), and the decay of this transverse component is measured, typically on the millisecond time scale. In order to suppress dephasing or other spin coherent effects, the experiments generally involve a spin-lock, which has the desired effect of refocusing evolution of the isotropic chemical shift; in this way, in the absence of polymer dynamics, the magnetization would persist for very long times. For proteins, these measurements are made more incisive yet, by joining this relaxation experiment to additional chemical shift dimensions so that the magnetization from individual nuclei can be spectrally resolved, and dynamics information is obtained for individual nuclei in specific amino acids, in parallel for many sites in the molecule. Apart from the promise of biophysical insights, measuring rotating frame relaxation ($R_{1\rho}$) is of practical interest to the spectroscopist. Like transverse relaxation (R_2), rotating frame relaxation ($R_{1\rho}$) governs the detection efficiency in a number of pulse sequences that involve spin-locks to effect magnetization transfer or to simplify (edit or decouple) the spectrum.

2. DESCRIPTION OF $R_{1\rho}$ IN SOLID STATE NMR

Rotating frame relaxation measurements for solids are broadly reminiscent of the analogous measurements carried out in solution, which is a popular and mature experimental strategy for characterizing dynamics of soluble proteins.[6,7] Due to advances in theory, software, hardware, pulse sequences, and sample preparations, solid state NMR (SSNMR) has seen continued growth as a tool for biopolymer studies leading to highly resolved multidimensional correlation spectra. Naturally, this has led to the exploration of analogous rotating frame relaxation experiments in solid state NMR. Many parallels exist in the applications of these methods for solids and solution. As for the case of solution NMR, rotating frame relaxation measurements are in some cases combined with other relaxation techniques, in particular R_1, to probe a larger range of time scales, from picoseconds to microseconds, and elucidate multiple motions that contribute to the measurements. In both cases, extension of these measurements to include multiple experimental temperature points allows for the extraction of an energy of activation for the analyzed processes. For both solution and solid state NMR, there is a fertile interdisciplinary opportunity when experimental NMR studies are combined with computational molecular dynamics.

There are also numerous distinctions between solution and solid state NMR relaxation measurements. Solid state NMR $R_{1\rho}$ relaxation measurements are expected to have a somewhat more extended time scale of sensitivity; this is because for solid state NMR the changes in the local field that drive relaxation tend to be larger since they include the anisotropic contribution mentioned above. Also, the combination of the spin-lock with magic angle spinning during the relaxation period leads to a number of complexities and opportunities that exist for solid state NMR but not solution NMR, which are explored in this article.

Perhaps the most important distinction between solution and solid state NMR dynamics measurements is the range of applicability. Without a requirement for crystallization or limitations for molecular weight, solid state NMR is applied in situations where many traditional methods would not be applicable, for example, where limited molecular tumbling of the molecule precludes the study by solution state NMR. Figure 1 highlights the breadth of the biological systems, from crystalline globular proteins to amyloid fibrils and oligomeric systems to complex membrane proteins, that have been studied using solid state $R_{1\rho}$ relaxation. Early solid state $R_{1\rho}$ relaxation studies explored well behaved globular proteins, in a microcrystalline state, e.g., ubiquitin and GB1. Additional studies have

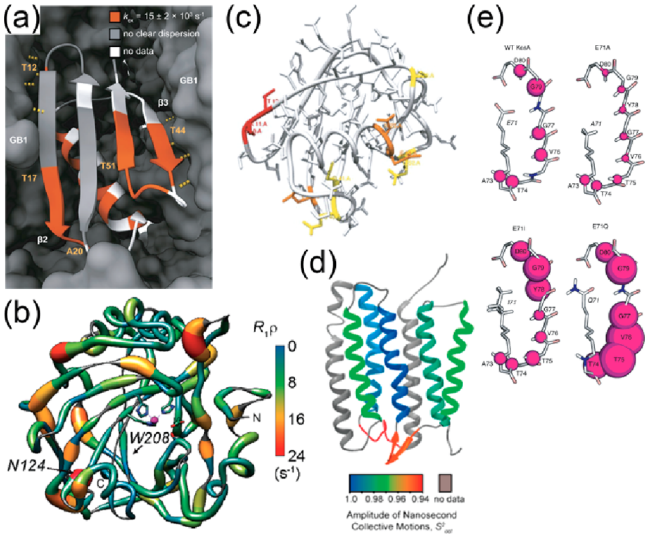

Figure 1. Ribbon diagrams demonstrating the residue specific results of solid state NMR rotating frame relaxation studies of various globular proteins (a) GB1 (adapted from ref 9; Copyright 2019 Springer Nature under a Creative Commons (CC-BY 4.0) license http://creativecommons.org/licenses/by/4.0/), (b) hCAII (adapted with permission from ref 26; Copyright 2018 American Chemical Society), and (c) UBQ (adapted with permission from ref 20; Copyright 2017 Wiley), and membrane proteins. (d) ASR (adapted with permission from ref 8; Copyright 2017 American Chemical Society) and (e) KcsA (adapted from ref 25; Copyright 2019 Springer Nature under a Creative Commons (CC-BY 4.0) license http://creativecommons.org/licenses/by/4.0/).

https://doi.org/10.1021/acs.chemrev.2c00442
Chem. Rev. 2022, 122, 14940−14953

Table 1. Some Applications Demonstrating Rotating Frame Relaxation for Detecting Protein Motion by SSNMR with the Fit Time Scales (τ_c) and Squared Order Parameters (S^2)/Populations Taken from Either Model Free or Bloch McConnell Fittings of the Data Shown[a]

	nuclei			measurement			fit motion #1: MF or Bloch McConnell (BM)	fit motion #2/3: MF
protein	^{15}N	^{13}C	^{1}H	$R_{1\rho}$	R_1	# of points	τ_c (p/S^2)	τ_c (p/S^2)
ASR[8]	X			X	X	4−5	sub μs ($S^2 \approx 0.89-0.99$)	sub ns ($S^2 \approx 0.89-0.99$)
GB1[9]	X			X		10+	67 μs	
UBQ[20]	X			X		3	0.5−3 μs ($S^2 > 0.95$)	20−200 ps ($S^2 \approx 0.65-0.95$)
KcsA[25]	X			X		1	n.a.	
hCAII[26]	X			X		1	n.a.	
SH3[5]	X			X		10+	170 μs (p = 22%) − BM	294 μs (p = 51%), 297 μs (p = 8%) − BM
[b]SH3[27]	X			X		1	n.a.	
UBQ[28]	X			X		3+	340 μs (p = 9.3%) − BM	
ASR[29]	X			X		4	15−20 ns ($S^2 \approx 0.75-0.999$)	
GB1[31]	X			X	X	3+	80 μs ($S^2 > 0.98$)	
GB1[30]	X	X		X	X	2	50 ns ($S^2 \approx 0.9-0.99$)	10−100 ps ($S^2 \approx 0.6-0.9$)
HET-s[10]	X	X		X	X	3+	^{15}N 14.7 μs ($S^2 \approx 0.8-0.9$)/^{13}C 8.7 μs ($S^2 \geq 0.98$)	∼10^{-8} (S^2 = 0.7−0.99) and 10^{-10} s (S^2 = 0.8−0.99)
KcsA[11]	X			X		1	n.a.	
KpOmpA[12]	X			X	X	1	n.a.	
UBQ[13]	X			X		3+	∼10−99 μs ($S^2 > 0.9$)	
UBQ[14]	X		X	X		3	n.a.	
Y145Stop Prion protein[15]	X			X		3+	1 ms (p = 2%)	100−300 us (p ≈ 5−15%)
TET2 enzyme[32]		X		X		3+	6−55 ns (ortho-C, MF, S^2 = 0.4375)	85−110 μs (para-C, BM)
[b]Y145Stop Prion protein[16]	X	X		X		1	n.a.	
[b]SH3[17]	X			X		2	5−70 ns ($S^2 \approx 0.65-0.99$)	
UBQ[18]	X			X		1	n.a.	
hCAII[19]	X			X		7−10+	10−800 μs ($S^2 > 0.9$)	
[b]SH3[21]	X		X	X	X	3+	^{15}N: 5−360 μs ($S^2 > 0.925$)/^{1}H: 63 μs ($S^2 \approx 0.4-0.8$)	
NS4B[22]	X		X	X		1	n.a.	
GB1[23]	X	X		X		1	n.a.	
HBV[24]	X			X	X	4+	∼100 ns −30 μs	∼0.1−10 ns

[a]See section 5.1 for definitions of τ_c and S. [b]Studies that include rotating frame relaxation acquired with moderate MAS spinning (≤25 kHz).

further applied the use of ^{15}N $R_{1\rho}$ relaxation to examine dynamics in amyloid fibrils and membrane proteins in lipid bilayers in addition to the crystalline protein applications.

3. SOLID STATE NMR $R_{1\rho}$ APPLICATIONS FOR BIOLOGICAL SYSTEMS

3.1. General Introduction to Solid State NMR $R_{1\rho}$ Studies

Table 1 enumerates many exciting recent applications of rotating frame relaxation to biological systems. This list highlights that there are many formats used for solid state rotating frame relaxation experiments. For example, the various nuclei (^{1}H, ^{15}N, or ^{13}C relaxation) have different opportunities and advantages for elucidating motions. One popular format for solid state $R_{1\rho}$ measurements of biopolymers involves amidic ^{1}H detected experiments which is an aspect of solid state NMR that has had many advances recently.[2] Commonly, these experiments involve recording the relaxation of the attached ^{15}N, for which angular fluctuations of the amide functional group would be expected to modulate both the anisotropic chemical shift of the amidic ^{15}N and the dipolar coupling to the directly attached proton.[8−31] Some studies additionally probe the relaxation of the detected ^{1}H.[14,21,22] In general, these studies are carried out at relatively high applied magnetic field strength (>700 MHz), use fast magic-angle spinning ($\nu_r \geq$ 50 kHz), and often also involve at least partial deuteration of the protein sample. With these conditions, protons can be detected with excellent sensitivity. Also, complicating effects from the evolution of spin−spin couplings and other kinds of unwanted coherent evolution are attenuated with the use of faster MAS. While some fast MAS equipment is commercially produced, and has become more broadly available, the applicable methods and best practices are still evolving.

3.2. Studies Probing $R_{1\rho}$ on ^{13}C Nuclei

A handful of other studies have probed the rotating frame relaxation of ^{13}C in biopolymers, extending the range of functional groups in the backbone and side chain that can be probed. ^{13}C relaxation can be driven by fluctuations in the chemical shift of the carbon (which exhibit anisotropies up to 100 ppm) as well as dipolar couplings to directly attached protons, with small additional contributions from other directly bonded spins (^{13}C, ^{15}N, or other). Promising studies of C-alpha,[10,16] carbonyl,[23,30] and aromatic[32] carbons in protein systems are among the examples listed in Table 1. The use of specific isotopic enrichment schemes to isolate the ^{13}C sites and eliminate strong homonuclear couplings is employed in some cases. Overall, there appears to be many aspects of these measurements yet to explore.

https://doi.org/10.1021/acs.chemrev.2c00442
Chem. Rev. 2022, 122, 14940−14953

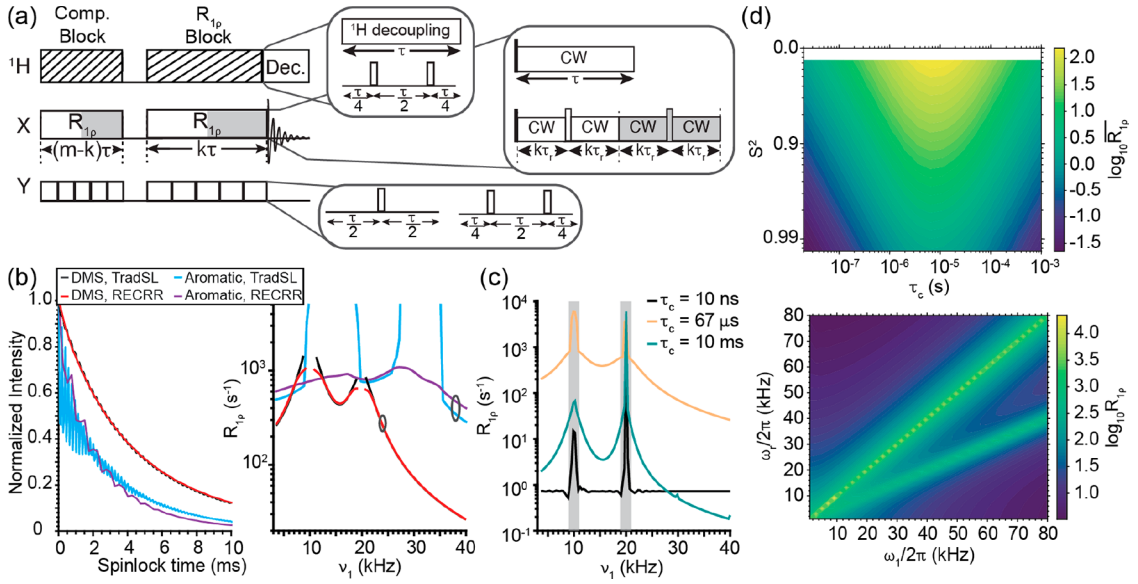

Figure 2. (a) Rotating frame relaxation pulse sequences illustrating various types of sequences that may be used on each channel during the spin-lock. (b) Numerically simulated time decays for traditional spin-lock (black and cyan) and RECRR (red and purple) experiments on two different systems, dimethyl sulfone or DMS (black and red) and a ortho ^{13}C on a symmetric aromatic group (cyan and purple) at $\nu_1 = 2.4\ \nu_r$ (b, left). Relaxation dispersion curves for the same systems and experiments (b, right); $R_{1\rho}$ rate constants were extracted by fitting the time decay to a single exponential function. The gray circle indicates the point depicted on the left. ^{13}C sites with highly anisotropic shielding in comparison with the spinning frequency, such as carbonyls and aromatic groups at moderate spinning frequencies, typically exhibit elevated relaxation and coherent dephasing, in comparison with sites with smaller anisotropy (such as methyl groups), as illustrated in b (cyan vs black). The RECRR sequence refocuses coherent evolution of the anisotropic shift, allowing the relaxation decay to be recorded with greater fidelity (purple curve as compared to the traditional spinlock in cyan). Simulations of DMS were performed at a static magnetic field of 400 MHz with a spinning frequency of 10 kHz with $\delta = -36.77$ ppm, $\eta = 0$, $\tau_c = 67\ \mu s$, and $\beta = 109°$ ($S^2 = 0.3295$), and simulations of aromatic carbon were performed at a static magnetic field of 750 MHz with a spinning frequency of 16 kHz, with $\delta = 175$ ppm, $\eta = 0$, $\tau_c = 700\ \mu s$, and $\beta = 120°$ ($S^2 = 0.4375$). (c) Numerically simulated $R_{1\rho}$ dispersion curves for DMS (computed using the same parameters as for (b) excepting τ_c) illustrating characteristic differences between fast limit ($\tau_c = 10$ ns), intermediate ($\tau_c = 67\ \mu s$), and slow limit ($\tau_c = 10$ ms) time scales. (d) Contour plots of the extracted $R_{1\rho}$ rate constant for numerical simulations of DMS with respect to the square of the order parameter (S^2) and the correlation time (τ_c) (top) and with respect to the applied spin-lock field ($\omega_1/2\pi$) and the spinning frequency ($\omega_r/2\pi$) (bottom). DMS simulations for the τ_c vs S^2 plot were performed with the following parameters: $\omega_{0H}/2\pi = 400$ MHz, $\nu_r = 10$ kHz, $\nu_1 = 2.55, 3.15, 3.55, 3.85, 4.2\ \nu_r$, $S^2 = 0.25-1.0$, $\delta = -36.77$ ppm, $\eta = 0$, $\tau_c = 10^{-8}$ to 10^{-3} s with the average rate constant, $\overline{R_{1\rho}}$, evaluated across the ν_1 dispersion curve. The DMS simulations for the $\omega_1/2\pi$ vs $\omega_r/2\pi$ plot were performed with the following parameters: $\omega_{0H}/2\pi = 400$ MHz, $\nu_r = 1-80$ kHz, $\nu_1 = 1-80$ kHz, $\beta = 109°$ ($S^2 = 0.3295$), $\delta = -36.77$ ppm, $\eta = 0$, $\tau_c = 67\ \mu s$.

4. EXPERIMENTAL APPROACHES

4.1. Traditional Spin-Lock Experiment

As for solution NMR, measuring the rotating frame relaxation of solid biological samples is typically achieved by applying a spin-lock on the nucleus of interest and monitoring the magnetization decay constant, i.e., the reduction in amplitude of a particular peak in a spectrum with respect to spin-lock duration, as illustrated in Figure 2a,b, and ordinarily this decay is fit to an exponential, to obtain the rotating frame relaxation rate constant, denoted as $R_{1\rho}$. The general and popular spin-lock pulse sequence element is relatively simple, wherein the spin-lock is achieved simply by continuous wave (CW) irradiation, herein referred as a traditional spin-lock (TradSL). A broad range of motion time scales from 10^3-10^7 s^{-1} cause readily detected elevations in the rotating frame relaxation rate, as illustrated in Figure 2d, making this experiment an excellent choice for detecting motion on the microsecond time scale.

4.2. Effect of Motions on Spin-Locked Nuclei

Given the broad range of motions that can result in relaxation, is it possible to determine the specific time scale from relaxation measurements? Notably, the plot of magnetization decay rate with respect to the motion's correlation time is "double-sided" (Figure 2d, top), sloping to smaller rates of decay with an increase in rate for fast limit motions and sloping to smaller rates of decay with a decrease in correlation times for slow limit motions. The term "fast limit" is defined by comparison of the rate constant k_{ex} to other characteristic frequencies involved in the experiment: $k_{ex} \gg \omega_1 + \omega_r$, where ω_1 is the applied field frequency and ω_r is the magic angle spinning frequency. The consequence of the "double-sided" dependence of rate with respect to correlation time is that comparative experiments that probe two temperatures or two closely related samples are ambiguous to interpret—an increase in relaxation rate constant could be owing to either decreased motional time scale (if the exchange is slow limit) or an increase in motional time scale (if the exchange is fast limit), absent additional information or assumptions. In fact, the increase could also be due to increase in angle or amplitude of the motion, as represented by the order parameter S, without a change of time scale. Identification of the exchange rate for the motion driving relaxation can be done by repeating the relaxation measurement at various spin-lock field strengths to obtain the plot of rotating frame relaxation rates as a function of applied field strength, which is referred to as a dispersion curve. The choice of spin-lock strengths is critical; since the spin-lock acts to refocus chemical shift evolution, the effects of exchange on time scales much slower than the refocusing time associated with the spin-lock strength are effectively suppressed. In practice, then, this strength is varied to

https://doi.org/10.1021/acs.chemrev.2c00442
Chem. Rev. 2022, 122, 14940−14953

generate a dispersion in the rate of decay that can be used to identify the time scale of the motion ("dispersion curve" analysis). As illustrated in Figure 2c, dispersion curves are flat for fast limit motion (10 ns) and strongly sloped when the motion is intermediate (67 μs) or slow (10 ms) exchange.[33] Both the sample spinning and the applied field can cause refocusing of chemical shift evolution of the spin, and both are variable and of the order 1−100 kHz (or mid-microsecond time scale). If spinning or pulse induced refocusing occurs on a time scale much faster than the motion, the effect of the motion is largely quenched. Therefore, slow motions are implicated if fast vs slow spinning, or strong vs weak applied fields cause a marked change in the relaxation rate. In summary, under favorable conditions, dispersion curves can provide a ready signature for millisecond vs nanosecond motions and even supply a potential approach for quantitative determination of time scale.

4.3. Effects of Magic Angle Spinning

Magic angle spinning introduces features in the dispersion that are unfamiliar from the solution NMR curve. Pronounced elevated features are seen at the sample rotation frequency and twice this frequency, which have mixed contributions from unwanted coherent evolution and from the fact that the motion contributions for slower motions are maximal at these frequencies; these effects are discussed more in section 4.4. The use of a dispersion curve, i.e., repeating the experiment with a minimum of two different spin-locking fields, solves this problem in principle and is very incisive in providing at least a qualitative indication of time scale regime, a fact that has been exploited also for solution NMR.

Measurements in solids have added experimental and theoretical complexity related to the sample rotation used to achieve high resolution solid state NMR spectra. The pulse used to refocus the magnetization may lead to more complex effects than for the solution experiments, and does not effectively suppress evolution of dipolar couplings and chemical shift anisotropy under many experimental conditions. For example, magic angle spinning has the effect of refocusing (or averaging) the evolution of the chemical shielding anisotropy. At first blush, this would seem to be powerful, to employ two independent measures, spinning and the spin-lock, to refocus coherent evolution. However, they interact in a coherent way, and, if the spin-lock field strength ω_1 is matched to the spinning frequency ω_r, the CSA does not refocus after each rotor period but rather undergoes significant net evolution, an effect referred to as "recoupling" or "reintroduction of the tensor".[34] Coherent evolution, defined for the purposes of this article as the evolution of coherent spin interactions during the application of a spin-lock, is therefore expected at these conditions, variously called CSA conditions or R^3 conditions, where $\omega_1 = n\omega_r$.

4.4. Minimizing Coherent Evolution

The requirement that there be no coherent evolution has been a bottleneck for some SSNMR $R_{1\rho}$ studies in practice because avoiding these specific "recoupling conditions" and others involving dipolar couplings is not as simple as one might initially think. The matching conditions are expected to unavoidably have a width of the order of the span of the anisotropy and so render many portions of the dispersion curve unsuited to relaxation analysis. Moreover, experimental artifacts such as spatial inhomogeneity in the RF field can lead to additional apparent broadening of these conditions in practice. The need to avoid conditions by a wide margin in order to avoid strong coherent evolution is demonstrated in Figure 2d, bottom. It requires in practice that the span of the CSA be small compared to the spinning frequency ω_r, that isotopic dilution be used (e.g., by deuteration and use of sparse ^{13}C or ^{15}N), and that recoupling conditions be avoided in the selection of spin-lock strength. Alternatively, special pulse sequences that refocus or defeat the recoupling can be adopted, as discussed below.

One remedy to avoid these conditions and their associated issues is to elevate the spinning frequency ω_r, and use relatively weak RF fields ω_1, in particular ensuring that the span of the CSA be small compared to the spinning frequency, and the difference $\omega_r - \omega_1 > \delta$. Dipolar driven coherent evolution is expected to be attenuated at high frequency spinning as well, removing another potential source of coherent evolution, though isotopic dilution can also be employed for this purpose. Furthermore, fast spinning has the additional benefit that it is compatible with ^1H detected experiments and relatively narrow ^1H lines, which in turn exhibit important advantages in detection sensitivity.[3] Therefore, some of the applications listed in Table 1 utilize higher spinning frequencies ($\nu_r \geq 50$ kHz).

Despite the advantage of high spinning frequencies described above, in many cases moderate spinning frequencies have been and continue to be utilized for $R_{1\rho}$ measurements together with direct ^{13}C detection. This can be motivated by practical considerations, namely, the availability of the equipment for this style of experiment, resulting in its being well tested and user-friendly. It is also noteworthy that the slower spinning frequency leads to increased sensitivity to intermediate time scale motions for many cases (stronger relaxation rates for the same motion and spin system). A strategy to address unwanted evolution of the CSA at lower spinning frequencies utilizes refocusing pulses during the spin-lock that effectively refocus numerous interactions so that net evolution is suppressed. For example, a pulsed spin-lock sequence element termed the REfocused CSA Rotating frame Relaxation (RECRR) suppresses evolution of the magnetization under the influence of the anisotropic CSA.[35] For anisotropic systems studies with moderate spinning frequencies, the improvement in detection sensitivity and precision of relaxation measurements using RECRR rather than a traditional spin lock is considerable, as illustrated in Figure 2.

For experiments at lower sample spinning frequencies, some dipolar driven coherent evolution can be avoided by use of sparse isotopic labeling schemes to isolate the spin system and simplify the measurement and its analysis. Also, various decoupling elements have been used on the ^1H and Y channels with the intention of suppressing dipolar evolution or to reduce cross-correlated relaxation involving both dipolar and CSA mechanisms. Frequently, this has been implemented in the form of one or two π pulses during the spin-lock time, as shown in Figure 2a. In some cases, high powered CW decoupling is applied on the ^1H channel while recording rotating frame relaxation on another channel (^{13}C), ideally with an amplitude (ν_{dec}) that avoids magnetization transfer or interference with a pulsed spin-lock element and ideally without interference between the decoupling and the motion of interest.[36] In some cases, a compensation block of length related to the rotor period is utilized to ensure that each time point during the decay has an identical total RF load (and associated RF heating) for the experiment. For complex biological systems, the relaxation measurement pulse sequence element is inserted into two- or three-dimensional experiments to create a pulse sequence that allows for site-specific measurements of the rotating frame relaxation rates.

https://doi.org/10.1021/acs.chemrev.2c00442
Chem. Rev. 2022, 122, 14940−14953

The efforts highlighted above point the way to possible future inventive pulse sequences that suppress a range of unwanted coherent effects, to best preserve magnetization (and result in better sensitivity) and render the relaxation measurements more accurate and precise.

5. ANALYSIS AND SIMULATION TO DETERMINE MOTION TIME SCALES

5.1. Model Free Analysis

Various analysis strategies have been attempted for obtaining conformation exchange characteristics from experimental NMR relaxation data. While qualitative indications of mobility can provide insights into biopolymer function and stability, the larger goal of these studies is to obtain quantitative constraints on structure changes and their time scales. A common approach to identifying the angle and time scale is model free analysis (MF). MF analysis involves analytic generalized equations derived from Bloch−Wangness−Redfield theory which were developed initially for biopolymer dynamics in solution.[37] These parsimonious expressions describe expected relaxation rates for a motion or several motions, each characterized by two parameters, a correlation time, τ_c, and an order parameter, S, that represents the amplitude of the motion. (Many recent NMR studies use the term S^2 as the order parameter; however, we adhere here to S representing a general order parameter and S^2 representing the square of this generalized order parameter; see section 5.2 for a more detailed description of how the order parameter is defined in NMR studies). The MF expressions are user-friendly in the sense that they are relatively simple, differentiable, and do not require knowledge of the type of motion. This approach has had a significant impact on solution NMR of biopolymers, and there are a number of software packages available.[38] The expressions are expected to be applicable only for a useful but circumscribed regime. The fast limit weak field approximations that are inherent to Redfield theory are assumed, suggesting that these expressions should only be applicable if the correlation time is much faster than the characteristic relaxation time (i.e., faster than the ms time scale) and faster than the inverse of the anisotropic interaction that causes relaxation (here faster than about 20 μs). If multiple motions are included, they should be separable mechanistically. The basic MF expressions also assume that the anisotropy driving the relaxation is uniaxial (cylindrically symmetric). The expressions do not account for any coherent evolution and so should be used to fit data where coherent evolution has been effectively suppressed.

5.2. Expressions for Model Free Analysis of Solid State NMR

Modified MF expressions were recently developed for magic angle spinning (MAS) SSNMR studies.[39] This approach provides relatively simple expressions for a relaxation process driven only by chemical shift anisotropy, as indicated below and a different set of equations for processes driven by fluctuations of the dipolar interaction. The expressions derived for model free prediction of rotating frame relaxation driven by the CSA interaction[39] and used in this study were as follows.

$$R_{1\rho}^{\mathrm{CSA}} = R_1^{\mathrm{CSA}} + \sin^2\theta_{\mathrm{p}}\left(R_{1\Delta}^{\mathrm{CSA}} - \frac{1}{2}R_1^{\mathrm{CSA}}\right) \tag{1}$$

here CSA refers to the chemical shielding mechanism, $R_{1\Delta}$ refers to exchange contributions to the transverse relaxation, R_1 represents other longitudinal decay rates, and θ_{p} refers to the tilt angle for the spin-lock.

$$R_1^{\mathrm{CSA}} = \frac{3}{4}(\delta\omega_{\mathrm{I}})^2 J_1(\omega_{\mathrm{I}}) \tag{2}$$

J_{m} refers to the spectral density associated with the motion, $\delta\omega_{\mathrm{I}}$ refers to the anisotropy of the CSA ($\sigma_{zz} - \sigma_{\mathrm{iso}}$, which in these expressions is approximated to be uniaxial, i.e., the asymmetry parameter $\eta = (\sigma_{yy} - \sigma_{\mathrm{xx}})/(\sigma_{zz} - \sigma_{\mathrm{iso}}) = 0$, though that approximation is not generally accurate).

$$R_{1\Delta}^{\mathrm{CSA}} = \frac{1}{6}(\delta\omega_{\mathrm{I}})^2\left(\frac{1}{2}J_0(\omega_{\mathrm{e}} - 2\omega_{\mathrm{r}}) + J_0(\omega_{\mathrm{e}} - \omega_{\mathrm{r}}) + J_0(\omega_{\mathrm{e}} + \omega_{\mathrm{r}}) + \frac{1}{2}J_0(\omega_{\mathrm{e}} - 2\omega_{\mathrm{r}})\right) \tag{3}$$

ω_{e} refers to the field strength of the RF excitation, and ω_{r} refers to the rotation frequency for magic angle spinning.

$$J_{\mathrm{m}}(\omega) = \frac{2}{5}(1 - S^2)\frac{\tau_{\mathrm{c}}}{1 + (\omega\tau_{\mathrm{c}})^2} \tag{4}$$

τ_{c} refers to the correlation function for the motion, and S represents the order parameter. S has a special definition for NMR studies, characterizing the degree of averaging for the operative tensor due to temporal fluctuations in the angle relating the director of the functional group to the applied static magnetic field. For uniaxially symmetric tensors, it can be expressed simply as the scalar ratio of the thermally averaged anisotropy to the corresponding static value $S = \langle\delta\rangle/\delta$ (angular brackets represent the time average). When generating a model free expression to represent a two-site hop Markov model with populations, p_{A} and p_{B}, and hop angle β, the following expression was used to compute the squared order parameter.[4,37]

$$S^2 = 1 + 3p_{\mathrm{A}}p_{\mathrm{B}}(\cos^2\beta - 1) \tag{5}$$

If the populations are assumed to be equal, as is the case for the numerical simulations here, the expression reduces to

$$S^2 = \frac{1}{4}(1 + 3\cos^2\beta) \tag{6}$$

In addition to the expressions above, R_1 and R_2 are frequently used, both experimentally and in analysis, to represent other longitudinal and transverse decay rates, respectively. R_1 and R_2 are assumed to be driven primarily by other motions that operate on nanosecond to picosecond time scales. R_1 and R_2 have also been approximated analogously by a model free expressions; for example, if the rate is driven by fluctuations in the CSA, R_1 takes the same form as eq 2, and $R_2 = \frac{1}{8}(\delta\omega_{\mathrm{I}})^2(4J_0(0) + 3J_1(\omega_{\mathrm{I}}))$, with spectral densities that are assumed to take the same functional form as given above; however, due to the differences in the spectral density arguments, it would be driven by a process with a shorter correlation time than the primary driver for $R_{1\Delta}$.

As for solution NMR MF analysis, the SSNMR MF expressions are computationally convenient: they are in principle applicable to arbitrary random motion mechanisms described by a generalized order parameter S and a characteristic correlation time τ_c, and they are simple expressions, rapid to evaluate, and amenable to differentiation, interpolation, and intuition. As such, they have been popular and have already been used in the analysis of a number of studies, as illustrated in Table 1. The assumptions listed above for solution NMR applications all apply here as well, namely, that no significant coherent

https://doi.org/10.1021/acs.chemrev.2c00442
Chem. Rev. 2022, 122, 14940−14953

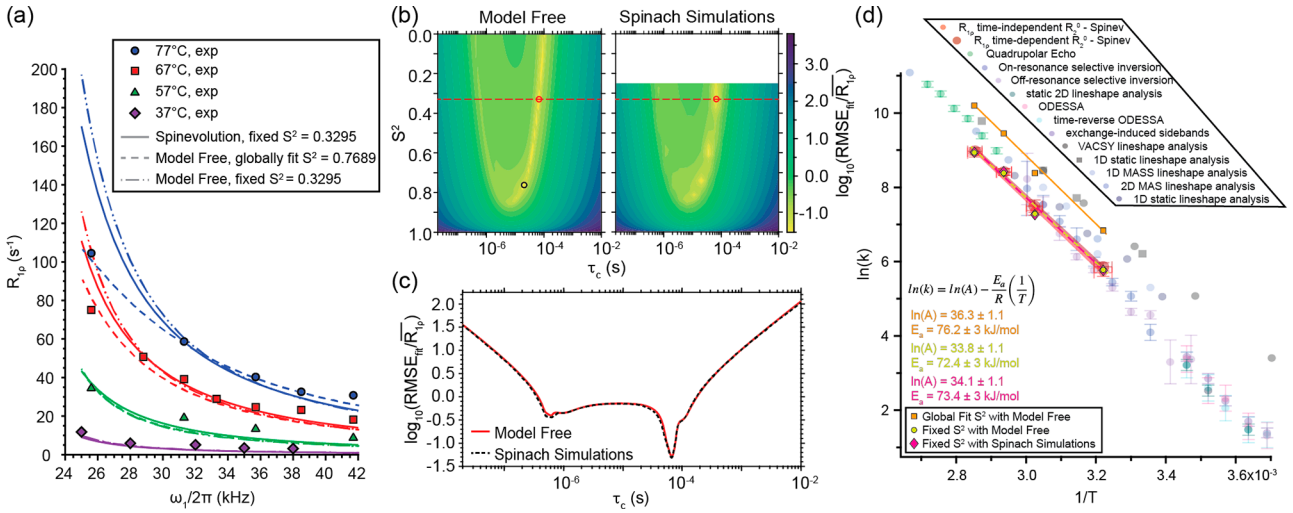

Figure 3. Model free and numerical simulation analysis results for DMS, including prior[43] and new results. Parameters for the simulations and experiments were $\omega_{0H}/2\pi$ = 400 MHz, ν_r = 10 kHz, ν_1 = 2.45, 2.75, 3.3, 3.55, 3.8, 4.2 ν_r, β = 109° (S^2 = 0.3295), δ = −36.77 ppm, η = 0 with a temperature independent R_2^0 included in the rate constant for each point. (a) Experimental (filled shapes), numerical simulation (solid lines), and model free (dashed and dot/dashed lines) relaxation dispersion curves for DMS. (b) Contour plots for the normalized RMSE of the 77 °C experimental data of the model free and numerical simulations[42] with the fixed S^2 best fit (red circle) and global S^2 best fit (black circle). The residuals for each point were used to calculate the $RMSE_{fit}$, which was then normalized by the average relaxation rate over the dispersion curve. (c) The slice at S^2 = 0.3295 for the model free and numerical simulations (correct value for the two-site hop). (d) Arrhenius plot for previous studies of DMS by various techniques[43] as well as the three new fits that were evaluated here (orange squares, yellow circles, and pink diamonds) along with their results for ln(A) and E_a. Note that the slope, and therefore the activation energy, is independent of the assumptions about the order parameter used for fitting (whereas the rates are quite dependent on the assumptions).

evolution should occur, a sometimes vexing point discussed in detail in section 4.4 and that the interactions should be uniaxial and the motions should be fast compared to the relaxation rates themselves and the interactions that drive them. If these requirements are met, MF can be a handy tool.

5.3. Use of Numerical Simulations for $R_{1\rho}$ Analysis

If the data do reflect contributions from coherent evolution, or if other assumptions regarding time scale fail, a more flexible and comprehensive approach is possible through numerical simulation of magnetization evolution under the influence of both coherent effects of the Hamiltonian(s) and chemical exchange in the form of an N-site hop mechanism. Numerical simulations in this context refers to solutions of the Stochastic Liouville Equations describing coherent evolution under the influence of the Hamiltonian with the added complexity that the spin is associated with a functional group undergoing conformational dynamics, described as an N-site Markoff process.[40] This calculation has been implemented in both SPINEVOLUTION[41] and SPINACH.[42] If all important interactions can be included, this approach is expected to be highly accurate and flexible, although computationally intensive. Several of the applications listed in Table 1 also employ this kind of strategy, or compare the two strategies. In the present examples, the Hamiltonian includes only an anisotropic chemical shielding (no dipolar couplings), the operative RF pulse sequence, and magic angle spinning; two sites of equal population are assumed, and the difference between the two sites is simply the orientation of the CSA with respect to the rotor, with no changes in the CSA values.

5.4. Implementation of Strategies for a Model System with Small CSA

5.4.1. MF vs Numerical Analysis of Experimental Data for a Model System. To explore the requirements that allow a unique and correct motional model to be identified from relaxation measurements, we analyzed data for which the motional model is assumed to be known, using both experimental data for a well characterized small molecule, as well as simulated dispersion curves that mimic perfect experimental data. We made simplifying assumptions, for example, the assumption that there is a single motion, which is assumed to be a two-site hop, wherein the direction of a uniaxial CSA interaction is modulated, with other interactions and causes of dephasing or relaxation omitted. We initially re-examined dimethyl sulfone (DMS), an experimentally forgiving system in the sense that the methyl carbon has a relatively small tensor, and when deuterated the CSA is a dominant term in the Hamiltonian driving relaxation. In previous studies,[43,44] NMR relaxation measurements on this system at several temperatures were used to extract the activation energy for a two-fold jump motion and associated change in the orientation of the chemical shift anisotropy (CSA) tensor of the methyl carbon. Analysis of these measurements carried out previously used the simulation program SPINEVOLUTION[41] identified an activation energy (E_a) of between 71 and 75 kJ/mol (Figure 3), in good agreement with prior analyses using various techniques characterizing thes activation energies as E_a = 63−87 kJ/mol. We reanalyzed those data and additional simulated data with an updated workflow, assuming no prior knowledge of rates, and thereby tested a protocol for future analysis of experimental data for new systems. The present analysis of these experimental data utilized the simulation package SPINACH[42] for numerical simulations as well as other routines in MATLAB including one for model free (e.g., Figures 2−7); notebooks with details for reproducing these simulations are available at the Web site for COMD/NMR at the New York Structural Biology Center (https://comdnmr.nysbc.org/comd-nmr-dissem/publications/2022_chemrev).

In Figure 3a, experimental relaxation rates as a function of the spin-lock strength $\omega_1/2\pi$ (aka dispersion curves) are compared to simulations based on different analysis methods used in the

https://doi.org/10.1021/acs.chemrev.2c00442
Chem. Rev. 2022, 122, 14940−14953

previous study.[43] This study illustrates that employing a dispersion curve and not a single relaxation point can make it possible to distinguish between slow, fast, and intermediate exchange motions, and to extract order parameters and correlation times.

5.4.2. Covariance between Correlation Time and Order Parameter. Proceeding to a quantitative analysis of the data set, it is noteworthy that the basin of acceptable fits shows clear covariance between the time scale and the order parameter. Indeed, one can anticipate that it should be impossible to uniquely determine τ_c and S from dispersion curves in either the fast limit or the slow limit kinetic regimes, based on MF expressions. In the fast limit, where $k_{ex} \gg \omega_1 + \omega_r$, we expect a family of equivalently good fits in which S and τ_c are covariant since the dependence of the relaxation rate on τ_c and S has the functional form $\tau_c\ (1 - S)^2$ throughout this kinetic regime (independent of B_0, ω_1, or ω_r), and no manipulation of experimental parameters will allow us to separate or determine unique solutions for S and τ_c. Similarly, for the slow limit, rates depend on $\frac{(1-S)^2}{\tau_c}$ and unique fits are not expected.

Based on the discussion above, one can conclude that prior knowledge of S or the hop angle for the motion is useful determining the time scale in the general case. A global minimum can be identified when the order parameter is fixed to the known value, and is in agreement for the two simulation approaches. For example, for some systems it can be intuited from assumptions about the mechanism of motion in highly symmetric systems. Alternatively, the order parameter can be experimentally determined from measurements of the averaged strength of the interaction that drives relaxation (the CSA or dipolar coupling), and comparison to the static value. For example, measurements of motionally averaged effective dipolar coupling constants have been reported in many cases.[45,46] The effect of motion on anisotropic interactions is frequently analyzed with the simplifying assumption of a single parameter $S = \langle\delta\rangle/\delta$, where the angle brackets represent the time average. Alternatively, in principle, a more nuanced analysis of the effects of motion could be inferred from detailed comparisons of the anisotropy and asymmetry of the tensors at high vs low temperatures.[47,48]

5.4.3. Restraining the Order Parameter. DMS is a case in point illustrating the power of restraining S to obtain the time scale of motion. For most of the data, the motion is in the slow limit, resulting in a large basin of comparably good fits, whereas assumed prior knowledge of S (or the hop angle and geometry) dramatically narrows the range of compatible time scales (Figure 3c). In Figure 3a, the solid line represents the curves of the best fit solution from numerical simulations as with parameters as provided in Quinn and McDermott,[43] the dashed line represents the best fit solution of the model free expressions assuming there is one squared global order parameter, S^2, for the four different temperature points but that this value (S^2) is not known and the dot/dashed line is the best fit solution for the points where the S^2 is fixed at so that $S^2 = 0.3295$ to correspond with $\beta = 109°$. While the dashed line results in a better overall fit for the highest temperature points, it produces an unphysical squared order parameter of 0.7689, which corresponds to an angle difference between the CSA tensors of the two methyl carbons of ∼34°. A more detailed investigation of the highest temperature data set (77 °C) is shown in Figure 3b showing the comparison of the full root-mean-square error (RMSE) surface of the model free expressions and the numerical simulations. The best fit of the model free expressions to the global model free order parameters is demonstrated with a black circle (global meaning all data sets at all temperatures were fit to the same order parameter). While the model free expressions and numerical simulations produce near identical fitting surfaces with this small CSA system, neither produces a global minimum corresponding to the known order parameter. In other words, if one assumes the hop angle or order parameter to be known (as done previously[42]), the correct rate can be readily identified, but in the absence of that knowledge a spurious minimum will be selected.

5.4.4. Extracting the Activation Energy from $R_{1\rho}$ Analysis. The above discussion of the benefit to prior knowledge of the order parameter refers mainly to the fast limit and the slow limit, and not to the intermediate exchange. A unique fit to accurate values for both S and the time scale are potentially possible in the intermediate exchange regime. The utility of such a fitting procedure to uniquely determine S and τ_c is somewhat hampered by the narrow range of applicable rates in intermediate exchange for which it is successful, making it fortuitous rather than a generally successful approach. Furthermore, peaks in intermediate exchange may be frequently weak, owing in part to the poor transfer efficiency in any pulse sequence that is sensitive to rotating frame relaxation or R_2 relaxation. Consequently, the fast limit and slow limit cases discussed above are of keen practical interest.

In many cases, the activation energy is of interest and is extracted from rates measured at different temperatures. For example, the energy obtained for DMS from rotating frame relaxation was in excellent agreement with prior reported values (Figure 3d). We explored the effect of the covariance of the order parameter and the time scale on our ability to determine the activation energy. We took the point of view that many motions will have a consistent or similar value for S across a finite temperature range, and that in global fitting S might be constrained to be consistent across temperature. If data were in the fast (or consistently in the slow) limit throughout the temperature range of interest, the effect of constraining S to an erroneous (but consistent) value results in best fit rates that are in error by a consistent multiplicative factor. In this case, when fit to the Arrhenius equation, a similar value for E_a will yield. In the example of DMS, activation energies of 73, 72, and 76 kJ/mol are obtained. Thus, a relatively consistent activation energy was obtained despite an error in the global order parameter and despite a consistent error in the best fit rates themselves (whereas the entropy of activation or pre-exponential factor would be expected to be in error).

The reason for a spurious preferred global fit absence of an order parameter restraint may in some cases be due to experimental imperfections that break the degeneracy of the basin of otherwise equivalent fits. For example, artifacts associated with coherent evolution appear in the dispersion curve and cause elevated relaxation rates in a broad range of applied field strengths near the spinning frequency. These features may result in a better fit with an intermediate exchange small angle motion even if the motion is in the fast or slow regime.

5.5. Extracting the Correct Correlation Time from Solid State NMR $R_{1\rho}$ Relaxation Dispersion Curves Using Model Free Analysis

Given that coherent evolution leads to spurious model free fits of the dispersion curve, we explored the benefit of using pulse sequences that suppress coherent evolution. Simulations for

https://doi.org/10.1021/acs.chemrev.2c00442
Chem. Rev. 2022, 122, 14940−14953

both the traditional spin-lock and RECRR experiments discussed above were tested against model free results. This was accomplished by extracting relaxation rates from a single exponential fit of the numerically simulated decay of magnetization and then comparing this relaxation rate to the model free expression. Two systems were used: the first was DMS (described above) with five ω_1 points between 2.45 and 3.8 ω_r, and the second was an aromatic-like carbon (meant to emulate a ring flip of a generic ortho aromatic carbon) with five ω_1 points from 0.43 and 2.33 ω_r (see Figure 4 for full details). With an assumed spinning frequency of 10 kHz, the methyl group of DMS has an anisotropy smaller than the spinning frequency, resulting in limited coherent evolution of the CSA during the spin-lock. By contrast, for the aromatic carbon, there is significant coherent evolution even with the spinning frequency of 16 kHz. Thus, these two cases illustrate two important regimes that may be encountered. Both systems were simulated assuming a range of correlation times (τ_{in} = 10 ns to 1 ms). The simulation assumed hop angles of β = 109° for DMS and 120° for the aromatic carbon. Resulting simulated data were fit both with and without the a priori knowledge of the order parameter. The results of the model free fits to traditional spin-lock experiments for the DMS system are shown in Figure 4a. The results displayed in Figure 4a demonstrate that model free expressions can determine the proper correlation time for traditional spin-lock experiments if the order parameter is known a priori and the anisotropy is comparable or smaller than the spinning frequency. Specifically, model free analysis for the methyl group of crystalline DMS yielded fit correlation times, τ_{fit}, within 20% of the initial correlation time, τ_{in}, for most of the simulated time scales. However, it is noteworthy that the ratio of the best fit τ_c to the initial τ_c (τ_{fit}/τ_{in}) deviates significantly from 1 (as does the order parameter) if the order parameter is not assumed to be known, outside of a limited range of τ_c (~1 order of magnitude centered around 10^{-5} s). This success for DMS is principally due to the small anisotropy, namely, that it is smaller than the spinning frequency, so that little coherent evolution takes place. Also, it is because there is a single dominant relaxation process (no dipolar couplings in this particular system). In this regime, both numerical simulations and model free expressions produce best fits with nearly identical relaxation rate constants, as illustrated in the inset of Figure 4a. Additionally, for small or moderate anisotropy systems (compared to the spinning frequency), RECRR and the traditional spin-lock result in comparable results.

By contrast, Figure 4b shows the results of fitting simulated data for an aromatic carbon undergoing ring flip, where an anisotropy that is larger as compared to the spinning frequency is assumed. These results demonstrate that, by contrast to smaller anisotropy systems like the methyl group of DMS (above), the larger anisotropy system produced fits that were frequently several orders of magnitude off from the correct (assumed/simulated) τ_c value. Specifically, with the traditional spin-lock, and absent a priori knowledge of the order parameter, the fits gave a unique minimum, but these minima were rarely within 20% of the correct value. For large anisotropy systems (here the aromatic carbon), the use of RECRR in place of the traditional spin-lock for the experiments, and a priori knowledge of the order parameter during data analysis, resulted in improved ability to discern the correct time scale with model free analysis. The inset of Figure 4b clearly demonstrates that RECRR outperforms the traditional spin-lock in terms of extending the domain of applicability of the model free formalism for anisotropic systems; the numerical simulations match the model free determined relaxation rate for a range of assumed correlation times, which is particularly evident for fast exchange where $\tau_c < 10^{-5}$ s. Overall, even including the improvements from RECRR, the normalized best fit RMSEs are larger than those found for a smaller anisotropy system and the precision for the derived correlation times correspondingly poorer.

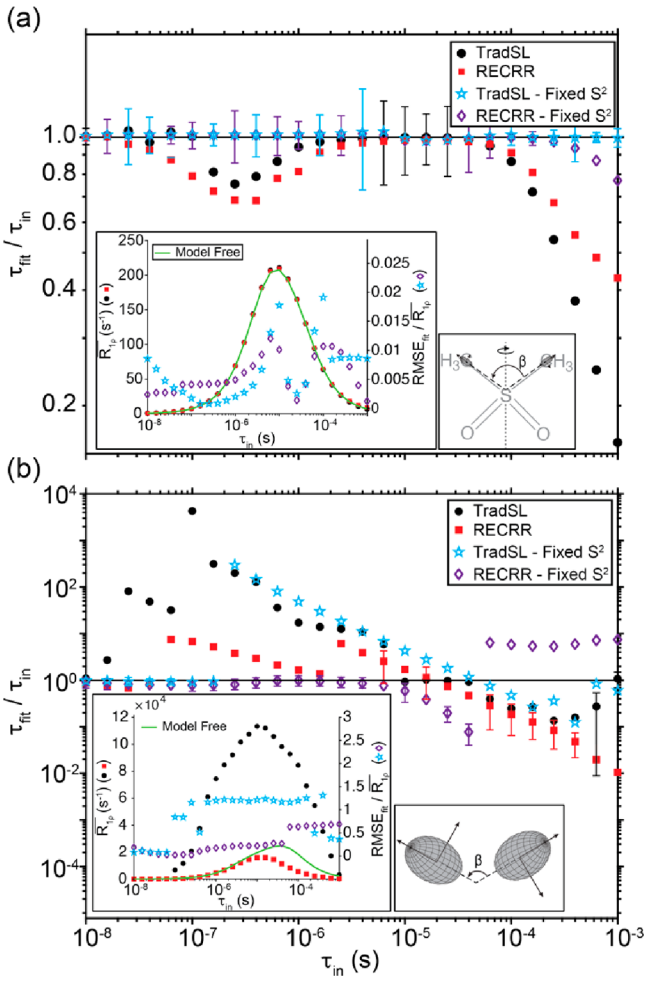

Figure 4. Comparison of the model free analysis best fit correlation time (τ_{fit}, y axis value) and the assumed/correct input correlation time of the numerical simulation (τ_{in}, x axis value) for DMS (a) and an aromatic-like carbon (b). Both the traditional spin-lock and RECRR experiments were simulated, and the model free fits were performed both with and without the a priori knowledge of S^2. The left inset shows the average relaxation rate ($R_{1\rho}$) for each simulated dispersion curve (averaged over all ω_1 points on the curve) and from the model free expressions (left axis). The right axis of the inset is the ratio of the best fit RMSE normalized with the average relaxation rate for the simulation. The inset for the aromatic carbon illustrates the better agreement of RECCR with MF expressions. The smallest error for each τ_{in} is shown, and errors are considerably larger in some cases. The right insets depict the two-fold hop motion of the simulation of DMS with the CSA tensor represented as an ellipsoid with its principal axis showing how the 180° hop leads to a β angle of 109°. For the theoretical aromatic carbon, the exchange of the ortho positions leads to a change of 120° for the CSA tensor axes. Details of the input system: DMS, $\omega_{0H}/2\pi$ = 400 MHz, ν_r = 10 kHz, ν_1 = 2.45, 2.75, 3.3, 3.55, 3.8ν_r, β = 109° (S^2 = 0.3295), δ = −36.77 ppm, η = 0 and aromatic carbon, $\omega_{0H}/2\pi$ = 750 MHz, ν_r = 16 kHz, ν_1 = 0.43, 0.63, 0.83, 2.16, and 2.33ν_r, β = 120° (S^2 = 0.4395), δ = 175 ppm, η = 0.

https://doi.org/10.1021/acs.chemrev.2c00442
Chem. Rev. 2022, 122, 14940−14953

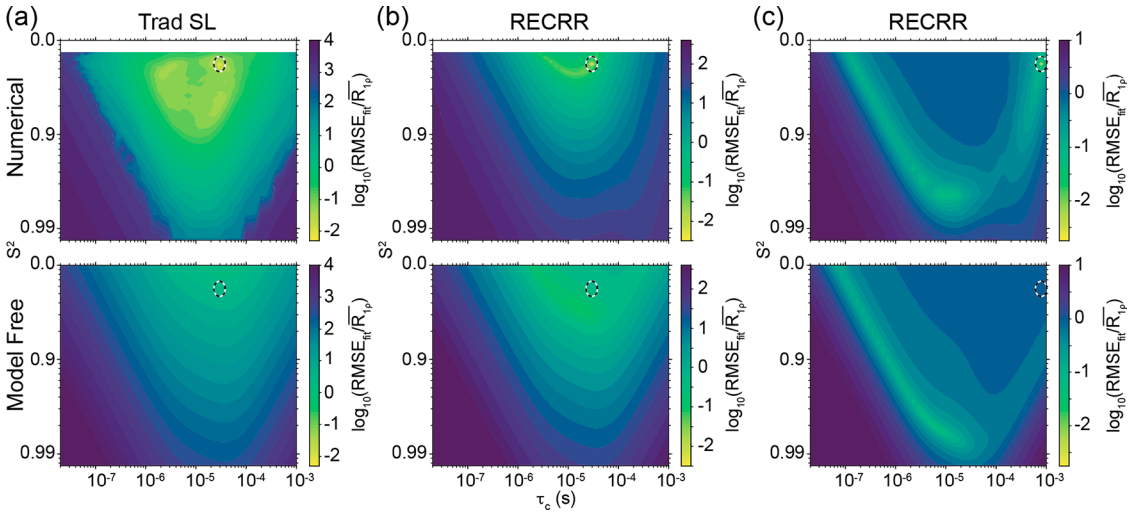

Figure 5. Evaluation of $R_{1\rho}$ dispersion curve analysis using extracted rate constants: Contour plots of the RMSE comparing a numerically simulated relaxation dispersion curve (CSA mechanism, aromatic carbon), for a traditional spin-lock (a) and RECRR (b, c) experiments. These simulated data were compared to a set of numerically simulated curves of varying correlation times and hop angles (top) or, separately, to model free expressions[39] (bottom). 1000 numerically simulated curves were evaluated with $\sigma = 0.10$ Gaussian random noise added to them before the residuals were calculated. The average of the residuals for each point were then used to calculate the $RMSE_{fit}$, which was then normalized by the average relaxation rate over the dispersion curve, $\overline{R_{1\rho}}$. The system parameters are $\delta_{CSA} = 175$ ppm, two-fold hop with $\beta = 120°$ and $\tau_c = 29.5$ (a, b) and 790 (c) μs; dispersion curve points $\omega_1 = 0.43$, 0.63, 0.83, 2.16, and 2.33 ω_r and spinning frequency $\nu_r = 16$ kHz. The black/white dashed oval indicates the correct values used in input parameters for the numerical simulation to create the "test data" relaxation dispersion curve being fit. Note that a more convergent minimum appears with numerical simulations (top) than for model free fitting (bottom). Also, significantly narrower basins of acceptable fits are seen for the RECRR experiments (b) vs the TradSL (a). If the RECRR experiment is fit using numerical simulations, the globally best fit returns the correct correlation time for a broad range of time scales, an aspect under further investigation elsewhere. The comparison of the two minima for the numerical simulations in (c) are $RMSE_{fit}/\overline{R_{1\rho}} = 2.82 \times 10^{-3}$ at 790 μs and $S^2 = 0.4375$ and $RMSE_{fit}/\overline{R_{1\rho}} = 5.89 \times 10^{-2}$ at 9.1 μs and $S^2 = 0.9774$.

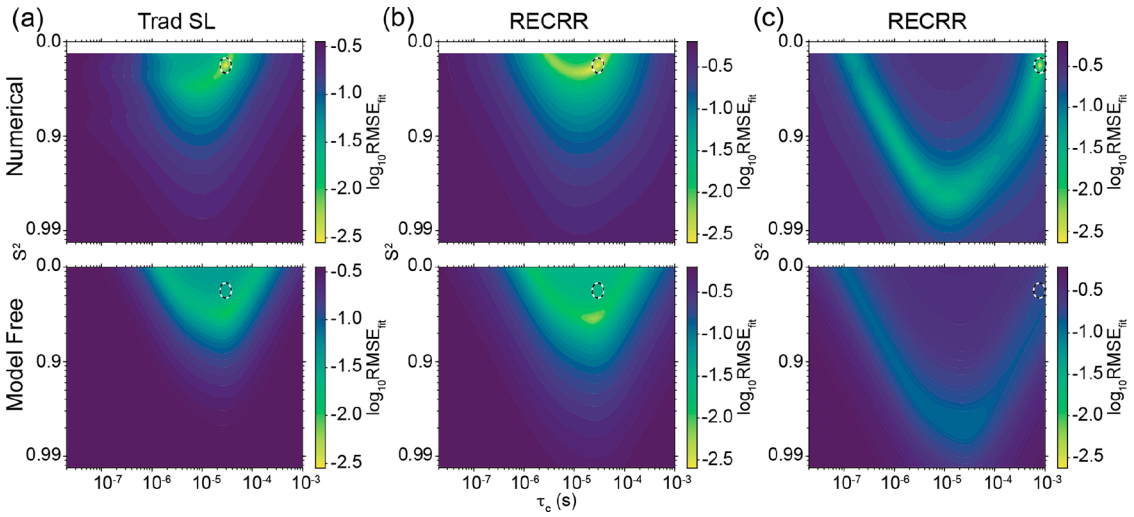

Figure 6. Evaluation of $R_{1\rho}$ dispersion curve analysis fitting time decays in the time domain (without fitting data to exponentials): Contour plots of the RMSE comparing the time decays of a numerically simulated relaxation dispersion curve (CSA mechanism, aromatic carbon), for a TradSL (a) and RECRR (b, c) experiments. These simulated data were compared to a set of numerically simulated curves of varying correlation times and hop angles with seven points (0, 0.25, 0.75, 1.25, 2.5, 4.375 (4.0, RECRR), 6.25 (6.0, RECRR) ms) (top) or, separately, to decays generated from the single exponential rate of model free expressions[39] for the same time points in the numerical simulations (bottom). 1000 numerically simulated curves were evaluated with $\sigma = 0.10$ Gaussian random noise added to them before the residuals were calculated. The average of the residuals for each point were then used to calculate the $RMSE_{fit}$. The system parameters are $\delta_{CSA} = 175$ ppm, two-fold hop with $\beta = 120°$ and $\tau_c = 29.5$ (a, b) and 790 (c) μs; dispersion curve points $\omega_1 = 0.43$, 0.63, 0.83, 2.16, and 2.33 ω_r and spinning frequency $\nu_r = 16$ kHz. The black/white dashed oval indicates the correct values used in input parameters for the numerical simulation to create the "test data" relaxation dispersion curve being fit. Note that a more convergent minimum appears with numerical simulations (top) than for model free fitting (bottom). While it appears a significantly narrower basin of acceptable fits is present in the TradSL (a) vs the RECRR (b) experiments this is due to the exact correct values of the anisotropic tensor being used in every simulation in the matrix allowing the coherent evolution present in the TradSL simulations to provide an additional vector for reducing the RMSE of the fit. If the RECRR experiment is fit using numerical simulations, the globally best fit returns the correct rate for a broad range of time scales, an aspect under further investigation elsewhere.

https://doi.org/10.1021/acs.chemrev.2c00442
Chem. Rev. 2022, 122, 14940−14953

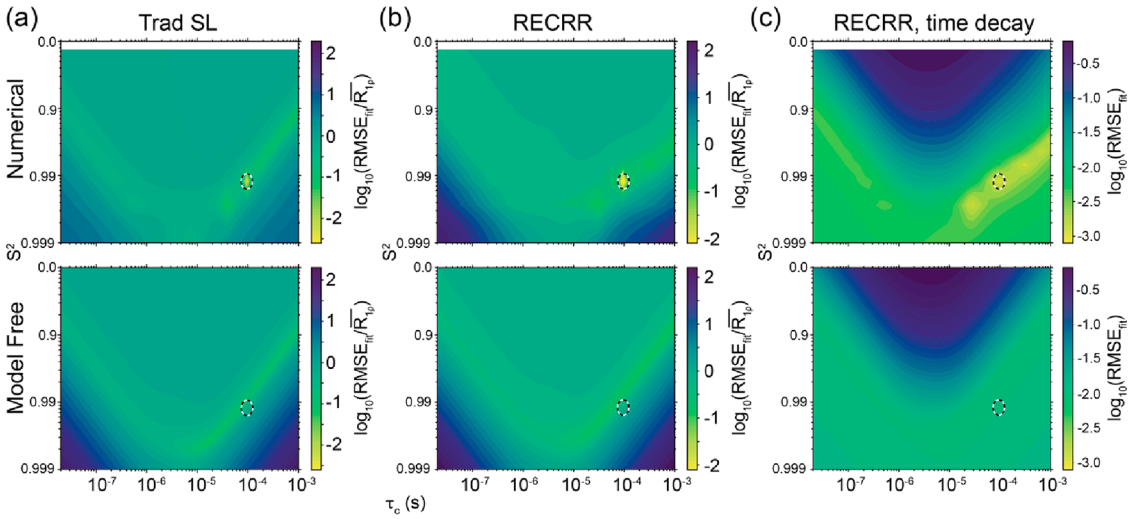

Figure 7. Evaluation of $R_{1\rho}$ dispersion curve analysis for ν_r = 60 kHz: Contour plots of the RMSE comparing a numerically simulated relaxation dispersion curve (CSA mechanism, carbonyl), for a traditional spin-lock (a) and RECRR (b, c) experiments for 900 MHz instrument (^{1}H frequency), assuming a magic angle spinning frequency ν_r = 60 kHz, and dispersion curve with ν_1 points at 10, 20, 35, 40, and 45 kHz, chosen to keep RF irradiation in realistic ranges and to avoid CSA matching conditions. The assumed values for the correlation time τ_c and squared order parameter S^2 were 95.4 μs and 0.9918 (6°) and are indicated with a black/white dashed oval. These simulated data were compared to a set of numerically simulated curves of varying correlation times and hop angles (top) or, separately, to model free expressions[39] (bottom). The data in (c) were compared to the time decays instead of the fitted relaxation rates. 1000 numerically simulated curves were evaluated with σ = 0.10 Gaussian random noise coadded before calculating residuals. A unique and correct fit can be obtained using numerical simulations, without prior knowledge of the angle or order parameter, whereas the fits via model free are incorrect and not unique due to the covariance of the fitting parameters. The minimum is similarly robust when using the time domain decay points in the place of the extracted relaxation rates. For the numerical simulation, the CSA tensor is defined as δ = −90 ppm and η = 0.6, and for the model free the CSA tensor is defined as δ = −90 ppm and η = 0.

5.6. Evaluating Solid State NMR $R_{1\rho}$ Relaxation Dispersion Curves by Model Free Analysis and Numerical Simulations

5.6.1. Analysis via Extracted $R_{1\rho}$ Relaxation Rate Constants. To address the difficulties with model free analysis for anisotropic systems highlighted above, numerical simulations of solid state NMR rotating frame relaxation experiments were also used as a data analysis tool. In this approach, a matrix of simulations employing the known spectroscopic parameters and assuming various angles and rates of the two-site jump model is compared with the experimental data. Figure 5 presents RMSE differences between normalized experimental decay constants and simulated decay constants, presented as a heatmap of unweighted contributions from all points on the dispersion curve. Loci of good agreement between simulation and experiment appear in yellow. An aromatic carbon undergoing two-site flipping is analyzed, with assumed time scales of τ_c = 29.5 (a and b) and 790 μs (c). Several conclusions are illustrated by these contour plots. The proper order parameter and time scale correspond to the global minimum of the numerical simulations for the RECRR experiments (b and c, top panel). This is not the case if model free analysis is used (b and c bottom panel) nor if the traditional spin-lock is used (a). If the order parameter is assumed to be known, the best agreement model free fits nevertheless do not correspond to the correct correlation time.

Additionally, if the order parameter is assumed to be known, the traditional spin-lock exhibits a broad minimum. These observations require further exploration to see if the RECRR and numerical simulations generally are a reliable approach. Meanwhile, at this stage, they provide optimism and motivation for using RECRR or similar experimental strategies and numerical simulations for studies of dynamics using anisotropic systems at moderate spinning frequencies.

Notably, incorrect MF fits for many cases wrongly return high order parameters (rigid) and intermediate exchange time scales (see Figure 5c, bottom for an example). This tendency may result from coherent evolution of the magnetization, which has the effect of broadening the rotary resonance conditions, resulting in dispersion curves that more resemble intermediate exchange time scale model free simulations than fast or slow limit model free simulations.

Other effects such as inhomogeneous RF fields may also lead to a similar systematic error.

5.6.2. Analysis via $R_{1\rho}$ Relaxation Time Decays. Additional fit precision can be afforded by simulating the decay curves in the time domain without fitting data to extract a rate constant (Figure 6). The decay curves are not in general strictly exponential, due to coherent evolution and relaxation anisotropic effects, and potentially effects of more complex kinetic models, and therefore avoiding the requirement that the data be fit to an exponential can improve the accuracy and precision of fitting.

5.6.3. Further Examination Using Faster Spinning. Faster MAS also presents a strategy for improving fidelity of data, as mentioned above, by removing coherent evolution. We examined a case of practical interest, the ^{13}C carbonyl measured with a MAS frequency of 60 kHz. Analogously to the studies described above, an aspect of interest is whether a dispersion curve (simulated, and therefore with known time scale and angles, and with realistic noise coadded) would have a unique and correct best model free fit. In Figure 7, a carbonyl carbon undergoing two-site flipping is analyzed, with an assumed time scale and order parameter of τ_c = 95.4 μs and S^2 = 0.9918 (6°). This analysis indicates that when evaluating a $R_{1\rho}$ dispersion curve, taken with five points below ν_r, when utilizing fast spinning on an environment with moderate CSA the TradSL and RECRR experiments are more similar than in the moderate

https://doi.org/10.1021/acs.chemrev.2c00442
Chem. Rev. 2022, 122, 14940−14953

spinning with large CSA case. However, most notably the model free evaluation of the data leads to a strong covariance between the fitted τ_c and S^2 demonstrating a lack of clear minimum if the order parameter is unknown. Additionally, even when the order parameter is known, the minimum fails to fall in the correct position when using the model free expressions. The numerical simulations show a clear minimum at the correct point; however, there are additional minima that appear in covariant line in τ_c and S^2 space (Figure 7, top), but if the order parameter is known prior to fitting, the numerical simulation fit yields the expected result.

In many of the examples above, it is noted that slow exchange data can erroneously fit to an intermediate exchange motion with an order parameter near one when MF fitting is used, as illustrated in Figure 5c for example. This false choice of best fit occurs because experimental dispersion curves for all kinetic regimes can show broadened features near the rotor frequency (and double) that resemble intermediate exchange effects (as fit by MF), while in fact these broadened features are due to other artifacts such as coherent evolution and/or poor B1 homogeneity. Numerical simulations of the curves can better distinguish between slow exchange and intermediate exchange much more robustly as seen in Figure 6c.

Overall, the discussion above indicates some hope for extracting quantitative descriptions of motion from SSNMR rotating frame relaxation studies, with a number of important caveats highlighted, including suppression of coherent evolution, the use of appropriate simulation strategies, and in many cases prior estimates of the angle or order parameter. In this discussion, numerous simplifications were also imposed. Our analyses were restricted to an assumed single motion or correlation time. In many systems, more complex motions might be encountered, and fitting these motions will presumably require larger sets of data. Given the complexity of biopolymer motions, identifying strategies for correct and accurate decomposition of multiple motions represents an important challenge for the future. Looking to the future, we face the exciting challenge of harnessing the many new technical developments in solid state NMR to enable study complex dynamics.

6. CONCLUSIONS AND OUTLOOK

In light of the burgeoning number of applications of rotating frame relaxation in magic angle spinning solid state NMR experiments, we expect that there is a bright future for this area of spectroscopy. We explored approaches to analysis, focusing on systems with simple kinetics of exchange (two-site hop) where the chemical shift anisotropy provides the dominant mechanism. We conclude that a correct and precise time scale can be obtained if a number of criteria are met. Beyond the need for high signal-to-noise decay profiles for resolved and assigned peaks, we emphasized the need for suppression of coherent evolution. For this reason, for systems with large CSA, pulse sequences that suppress coherent evolution or ultrafast spinning are needed. If coherent evolution is not fully suppressed, numerical simulations may be required to obtain confident and correct information about the motions. When all of these criteria are met, for favorable systems near intermediate exchange ($\omega_1 + \omega_r \approx k_{ex}$) dispersion ($\omega_1$ dependent) data can be used to determine the time scale of motion. More generally, considering fast and slow limit cases, prior knowledge of the angle or order parameter is needed to determine the correlation time with confidence. This is illustrated with a case with relatively narrow shielding anisotropy compared to the spinning frequency (a methyl group), where model free based fitting protocols identified correct rate constants if S is constrained by knowledge of the molecular geometry (angles) of the motion. In the absence of prior knowledge, covariance of τ_c and S leads to numerous minima in data fitting. Nevertheless, despite the fact that the unique and correct fit cannot be obtained without prior knowledge of the order parameter, the activation energy can be obtained without any prior knowledge in many cases. Going forward, given the powerful developments in faster MAS spinning frequencies and other new technologies, there are many opportunities for this area of science.

ASSOCIATED CONTENT

Special Issue Paper

This paper is an additional review for *Chem. Rev.* **2022**, volume *122*, issue 10, "Biomolecular NMR Spectroscopy".

AUTHOR INFORMATION

Corresponding Author

Ann E. McDermott − *Department of Chemistry, Columbia University, New York, New York 10027, United States;* orcid.org/0000-0002-9249-1649; Email: aem5@columbia.edu

Author

Eric G. Keeler − *New York Structural Biology Center, New York, New York 10027, United States*

Complete contact information is available at: https://pubs.acs.org/10.1021/acs.chemrev.2c00442

Author Contributions

CRediT: **Eric G. Keeler** conceptualization, data curation, formal analysis, funding acquisition, investigation, methodology, project administration, software, validation, visualization, writing-original draft, writing-review & editing; **Ann E. McDermott** conceptualization, formal analysis, funding acquisition, investigation, methodology, project administration, resources, supervision, validation, visualization, writing-original draft, writing-review & editing.

Notes

The authors declare no competing financial interest.

Biographies

Eric G. Keeler is currently the solid state NMR scientist at the New York Structural Biology Center where he focuses on the study of molecular motions by solid state NMR. He first began studying solid state NMR investigating the structure of silicate glasses in the lab of Prof. Philip J. Grandinetti at The Ohio State University where he obtained his B.S. in Chemistry in 2012. He then obtained his Ph.D. in Physical Chemistry in 2017 from MIT under Prof. Robert G. Griffin where he worked to advance the use of oxygen-17 NMR in the study of biological solids. Subsequently, he worked in the laboratory of Prof. Ann McDermott at Columbia University where he was a NIH postdoctoral fellow studying the use of solid state NMR rotating frame relaxation experiments to probe molecular motions in membrane proteins.

Ann McDermott, Ronald and Esther Breslow Professor of Biological Chemistry and Chair of the Chemistry Department at Columbia University, develops and applies methods to probe the structure, flexibility, and function of proteins using magnetic resonance. Her group investigates allosteric regulation of potassium ion channels,

https://doi.org/10.1021/acs.chemrev.2c00442
Chem. Rev. 2022, 122, 14940−14953

which play crucial roles in diverse contexts, from bacteria to the human nervous system. They have also determined the structures and characterized the dynamics of amyloids whose formation is a critical step in cellular signaling in humans. On the basis of this research, she is the recipient of the Pure Award in Chemistry, the Eastern Analytic Symposium Award for Achievement in Magnetic Resonance, and the Gunther Laukien Award in NMR, and she is an elected member of both the American Academy of Arts and Sciences, and the National Academy of Sciences. Her research group has been supported by the National Institutes of Health, the National Science Foundation, the Department of Energy, the Sloan Research Foundation, and the Cottrell Research Foundation. She holds a B.Sc. from Harvey Mudd College and a Ph.D. from the College of Chemistry at U.C. Berkeley, where she worked with Kenneth Sauer and Melvin Klein, and postgraduate training at MIT and the Francis Bitter National Magnet Laboratory with Robert Griffin.

ACKNOWLEDGMENTS

E.G.K. was supported by a postdoctoral fellowship from the National Institutes of Health (NIH) (Grant No. GM135350). A.E.M. was supported by Grant No. GM088724 from the NIH and Grant No. 1913885 from the National Science Foundation. This work was also supported by the New York Structural Biology Center (NYSBC) with support from the Center on Macromolecular Dynamics by NMR Spectroscopy, a Biomedical Technology Research Resource (NIH Grant No. GM118302) and the Biomedical Technology Development and Dissemination Center (1RM1GM145397-01). The NYSBC is also supported by the Empire State Division of Science Technology and Innovation and the Office of Research Infrastructure Program (NIH Grant No. CO6RR015495). A.E.M. is a member of the NYSBC.

REFERENCES

(1) Schanda, P.; Ernst, M. Studying Dynamics by Magic-Angle Spinning Solid-State NMR Spectroscopy: Principles and Applications to Biomolecules. *Prog. Nucl. Magn. Reson. Spectrosc.* **2016**, *96*, 1−46.
(2) Rovó, P.; Linser, R. Microsecond Time Scale Proton Rotating-Frame Relaxation under Magic Angle Spinning. *J. Phys. Chem. B* **2017**, *121*, 6117−6130.
(3) Rovó, P. Recent Advances in Solid-State Relaxation Dispersion Techniques. *Solid State Nucl. Magn. Reson.* **2020**, *108*, 101665.
(4) Zumpfe, K.; Smith, A. A. Model-Free or Not? *Front. Mol. Biosci.* **2021**, *8*. DOI: 10.3389/fmolb.2021.727553
(5) Rovó, P.; Linser, R. Microsecond Timescale Protein Dynamics: A Combined Solid-State NMR Approach. *ChemPhysChem* **2018**, *19*, 34−39.
(6) Palmer, A. G.; Williams, J.; McDermott, A. Nuclear Magnetic Resonance Studies of Biopolymer Dynamics. *J. Phys. Chem.* **1996**, *100*, 13293−13310.
(7) Palmer, A. G.; Massi, F. Characterization of the Dynamics of Biomacromolecules Using Rotating-Frame Spin Relaxation NMR Spectroscopy. *Chem. Rev.* **2006**, *106*, 1700−1719.
(8) Good, D.; Pham, C.; Jagas, J.; Lewandowski, J. R.; Ladizhansky, V. Solid-State NMR Provides Evidence for Small-Amplitude Slow Domain Motions in a Multispanning Transmembrane α-Helical Protein. *J. Am. Chem. Soc.* **2017**, *139*, 9246−9258.
(9) Öster, C.; Kosol, S.; Lewandowski, J. R. Quantifying Microsecond Exchange in Large Protein Complexes with Accelerated Relaxation Dispersion Experiments in the Solid State. *Sci. Rep.* **2019**, *9*, 11082.
(10) Smith, A. A.; Testori, E.; Cadalbert, R.; Meier, B. H.; Ernst, M. Characterization of Fibril Dynamics on Three Timescales by Solid-State NMR. *J. Biomol. NMR* **2016**, *65*, 171−191.
(11) Medeiros-Silva, J.; Mance, D.; Daniëls, M.; Jekhmane, S.; Houben, K.; Baldus, M.; Weingarth, M. ^{1}H-Detected Solid-State NMR Studies of Water-Inaccessible Proteins In Vitro and In Situ. *Angew. Chemie - Int. Ed.* **2016**, *55*, 13606−13610.
(12) Saurel, O.; Iordanov, I.; Nars, G.; Demange, P.; Le Marchand, T.; Andreas, L. B.; Pintacuda, G.; Milon, A. Local and Global Dynamics in Klebsiella Pneumoniae Outer Membrane Protein a in Lipid Bilayers Probed at Atomic Resolution. *J. Am. Chem. Soc.* **2017**, *139*, 1590−1597.
(13) Kurauskas, V.; Izmailov, S. A.; Rogacheva, O. N.; Hessel, A.; Ayala, I.; Woodhouse, J.; Shilova, A.; Xue, Y.; Yuwen, T.; Coquelle, N.; Colletier, J.-P.; Skrynnikov, N. R.; Schanda, P. Slow Conformational Exchange and Overall Rocking Motion in Ubiquitin Protein Crystals. *Nat. Commun.* **2017**, *8*, 145.
(14) Gauto, D. F.; Hessel, A.; Rovó, P.; Kurauskas, V.; Linser, R.; Schanda, P. Protein Conformational Dynamics Studied by ^{15}N and ^{1}H $R_{1\rho}$ Relaxation Dispersion: Application to Wild-Type and G53A Ubiquitin Crystals. *Solid State Nucl. Magn. Reson.* **2017**, *87*, 86−95.
(15) Shannon, M. D.; Theint, T.; Mukhopadhyay, D.; Surewicz, K.; Surewicz, W. K.; Marion, D.; Schanda, P.; Jaroniec, C. P. Conformational Dynamics in the Core of Human Y145Stop Prion Protein Amyloid Probed by Relaxation Dispersion NMR. *ChemPhysChem* **2019**, *20*, 311−317.
(16) Helmus, J. J.; Surewicz, K.; Surewicz, W. K.; Jaroniec, C. P. Conformational Flexibility of Y145stop Human Prion Protein Amyloid Fibrils Probed by Solid-State Nuclear Magnetic Resonance Spectroscopy. *J. Am. Chem. Soc.* **2010**, *132*, 2393−2403.
(17) Lewandowski, J. R.; Sass, H. J.; Grzesiek, S.; Blackledge, M.; Emsley, L. Site-Specific Measurement of Slow Motions in Proteins. *J. Am. Chem. Soc.* **2011**, *133*, 16762−16765.
(18) Kurauskas, V.; Weber, E.; Hessel, A.; Ayala, I.; Marion, D.; Schanda, P. Cross-Correlated Relaxation of Dipolar Coupling and Chemical-Shift Anisotropy in Magic-Angle Spinning R_1 NMR Measurements: Application to Protein Backbone Dynamics Measurements. *J. Phys. Chem. B* **2016**, *120*, 8905−8913.
(19) Singh, H.; Vasa, S. K.; Jangra, H.; Rovó, P.; Päslack, C.; Das, C. K.; Zipse, H.; Schäfer, L. V.; Linser, R. Fast Microsecond Dynamics of the Protein-Water Network in the Active Site of Human Carbonic Anhydrase II Studied by Solid-State NMR Spectroscopy. *J. Am. Chem. Soc.* **2019**, *141*, 19276−19288.
(20) Lakomek, N.-A.; Penzel, S.; Lends, A.; Cadalbert, R.; Ernst, M.; Meier, B. H. Microsecond Dynamics in Ubiquitin Probed by Solid-State ^{15}N NMR Spectroscopy $R_{1\rho}$ Relaxation Experiments under Fast MAS (60−110 kHz). *Chem. - A Eur. J.* **2017**, *23*, 9425−9433.
(21) Rovó, P.; Smith, C. A.; Gauto, D.; De Groot, B. L.; Schanda, P.; Linser, R. Mechanistic Insights into Microsecond Time-Scale Motion of Solid Proteins Using Complementary ^{15}N and ^{1}H Relaxation Dispersion Techniques. *J. Am. Chem. Soc.* **2019**, *141*, 858−869.
(22) Jirasko, V.; Lakomek, N. A.; Penzel, S.; Fogeron, M. L.; Bartenschlager, R.; Meier, B. H.; Böckmann, A. Proton-Detected Solid-State NMR of the Cell-Free Synthesized α-Helical Transmembrane Protein NS4B from Hepatitis C Virus. *ChemBioChem.* **2020**, *21*, 1453−1460.
(23) Tognetti, J.; Trent Franks, W.; Gallo, A.; Lewandowski, J. R. Accelerating ^{15}N and ^{13}C R_1 and $R_{1\rho}$ Relaxation Measurements by Multiple Pathway Solid-State NMR Experiments. *J. Magn. Reson.* **2021**, *331*, 107049.
(24) Malär, A. A.; Callon, M.; Smith, A. A.; Wang, S.; Lecoq, L.; Pérez-Segura, C.; Hadden-Perilla, J. A.; Böckmann, A.; Meier, B. H. Experimental Characterization of the Hepatitis B Virus Capsid Dynamics by Solid-State NMR. *Front. Mol. Biosci.* **2022**, *8*, 1−15.
(25) Jekhmane, S.; Medeiros-Silva, J.; Li, J.; Kümmerer, F.; Müller-Hermes, C.; Baldus, M.; Roux, B.; Weingarth, M. Shifts in the Selectivity Filter Dynamics Cause Modal Gating in K+ Channels. *Nat. Commun.* **2019**, *10*, 123.
(26) Vasa, S. K.; Singh, H.; Rovó, P.; Linser, R. Dynamics and Interactions of a 29 KDa Human Enzyme Studied by Solid-State NMR. *J. Phys. Chem. Lett.* **2018**, *9*, 1307−1311.
(27) Krushelnitsky, A.; Zinkevich, T.; Reif, B.; Saalwächter, K. Slow Motions in Microcrystalline Proteins as Observed by MAS-Dependent ^{15}N Rotating-Frame NMR Relaxation. *J. Magn. Reson.* **2014**, *248*, 8−12.

(28) Ma, P.; Haller, J. D. D.; Zajakala, J.; Macek, P.; Sivertsen, A. C. C.; Willbold, D.; Boisbouvier, J.; Schanda, P. Probing Transient Conformational States of Proteins by Solid-State $R_{1\rho}$ Relaxation-Dispersion NMR Spectroscopy. *Angew. Chemie - Int. Ed.* **2014**, *53*, 4312−4317.
(29) Good, D. B.; Wang, S.; Ward, M. E.; Struppe, J.; Brown, L. S.; Lewandowski, J. R.; Ladizhansky, V. Conformational Dynamics of a Seven Transmembrane Helical Protein Anabaena Sensory Rhodopsin Probed by Solid-State NMR. *J. Am. Chem. Soc.* **2014**, *136*, 2833−2842.
(30) Lamley, J. M.; Lougher, M. J.; Sass, H. J.; Rogowski, M.; Grzesiek, S.; Lewandowski, J. R. Unraveling the Complexity of Protein Backbone Dynamics with Combined ^{13}C and ^{15}N Solid-State NMR Relaxation Measurements. *Phys. Chem. Chem. Phys.* **2015**, *17*, 21997−22008.
(31) Lamley, J. M.; Öster, C.; Stevens, R. A.; Lewandowski, J. R. Intermolecular Interactions and Protein Dynamics by Solid-State NMR Spectroscopy. *Angew. Chemie - Int. Ed.* **2015**, *54*, 15374−15378.
(32) Gauto, D. F.; Macek, P.; Barducci, A.; Fraga, H.; Hessel, A.; Terauchi, T.; Gajan, D.; Miyanoiri, Y.; Boisbouvier, J.; Lichtenecker, R.; Kainosho, M.; Schanda, P. Aromatic Ring Dynamics, Thermal Activation and Transient Conformations of a 468 KDa Enzyme by Specific Labeling and Fast-MAS NMR. *J. Am. Chem. Soc.* **2019**, *141*, 11183.
(33) Krushelnitsky, A.; Reichert, D.; Saalwächter, K. Solid-State NMR Approaches to Internal Dynamics of Proteins: From Picoseconds to Microseconds and Seconds. *Acc. Chem. Res.* **2013**, *46*, 2028−2036.
(34) Gan, Z.; Grant, D. M.; Ernst, R.R. NMR Chemical Shift Anisotropy Measurements by RF Driven Rotary Resonance. *Chem. Phys. Lett.* **1996**, *254*, 349−357.
(35) Keeler, E. G.; Fritzsching, K. J.; McDermott, A. E. Refocusing CSA during Magic Angle Spinning Rotating-Frame Relaxation Experiments. *J. Magn. Reson.* **2018**, *296*, 130−137.
(36) Long, J. R.; Sun, B. Q.; Bowen, A.; Griffin, R. G. Molecular Dynamics and Solid State NMR. *J. Am. Chem. Soc.* **1994**, *116*, 11950−11956.
(37) Lipari, G.; Szabo, A. A Model-Free Approach to the Interpretation of Nuclear Magnetic Resonance Relaxation in Macromolecules. 1. Theory and Range of Validity. *J. Am. Chem. Soc.* **1982**, *104*, 4546−4559.
(38) Beckwith, M. A.; Erazo-Colon, T.; Johnson, B. A. RING NMR Dynamics: Software for Analysis of Multiple NMR Relaxation Experiments. *J. Biomol. NMR* **2021**, *75*, 9−23.
(39) Kurbanov, R.; Zinkevich, T.; Krushelnitsky, A. The Nuclear Magnetic Resonance Relaxation Data Analysis in Solids: General R_1/$R_{1\rho}$ Equations and the Model-Free Approach. *J. Chem. Phys.* **2011**, *135*, 184104.
(40) Vega, A. J.; Fiat, D. Relaxation Theory and the Stochastic Liouville Equation. *J. Magn. Reson.* **1975**, *19*, 21−30.
(41) Veshtort, M.; Griffin, R. G. SPINEVOLUTION: A Powerful Tool for the Simulation of Solid and Liquid State NMR Experiments. *J. Magn. Reson.* **2006**, *178*, 248−282.
(42) Hogben, H. J.; Krzystyniak, M.; Charnock, G. T. P.; Hore, P. J.; Kuprov, I. Spinach - A Software Library for Simulation of Spin Dynamics in Large Spin Systems. *J. Magn. Reson.* **2011**, *208*, 179−194.
(43) Quinn, C. M.; McDermott, A. E. Quantifying Conformational Dynamics Using Solid-State $R_{1\rho}$ Experiments. *J. Magn. Reson.* **2012**, *222*, 1−7.
(44) Quinn, C. M.; McDermott, A. E. Monitoring Conformational Dynamics with Solid-State $R_{1\rho}$ Experiments. *J. Biomol. NMR* **2009**, *45*, 5−8.
(45) Hong, M.; Yao, X. L.; Jakes, K.; Huster, D. Investigation of Molecular Motions by Lee-Goldburg Cross-Polarization NMR Spectroscopy. *J. Phys. Chem. B* **2002**, *106*, 7355−7364.
(46) Chevelkov, V.; Fink, U.; Reif, B. Accurate Determination of Order Parameters from ^{1}H,^{15}N Dipolar Couplings in MAS Solid-State NMR Experiments. *J. Am. Chem. Soc.* **2009**, *131*, 14018−14022.
(47) Solum, M. S.; Zilm, K. W.; Michl, J.; Grant, D. M. Carbon-13 Line Shape Study of Two-Site Exchange in Solid Dimethyl Sulfone. *J. Phys. Chem.* **1983**, *87*, 2940−2944.
(48) Hallock, K. J.; Lee, D. K.; Ramamoorthy, A. The Effects of Librations on the ^{13}C Chemical Shift and ^{2}H Electric Field Gradient Tensors in β-Calcium Formate. *J. Chem. Phys.* **2000**, *113*, 11187−11193.

https://doi.org/10.1021/acs.chemrev.2c00442
Chem. Rev. 2022, 122, 14940−14953